

1 | **Measurement of ~~Light~~ light absorbing particles in surface snow**  
2 | **of central and western Himalayan glaciers: spatial variability,**  
3 | **radiative impacts, and potential source regions**

Formatted: Highlight

4  
5  
6 Chaman Gul<sup>1,2,3,4</sup>, Shichang Kang<sup>1,4</sup>, Siva Praveen Puppala<sup>2</sup>, Xiaokang Wu<sup>5</sup>, Cenlin He<sup>6</sup>,  
7 Yangyang Xu<sup>5</sup>, Inka Koch<sup>1</sup>, Sher Muhammad<sup>1</sup>, Rajesh Kumar<sup>6</sup>, Getachew Dubache<sup>3</sup>

8 <sup>1</sup>State Key Laboratory of Cryosphere Science, Northwest Institute of Eco-Environment and Resources, Chinese  
9 Academy of Sciences, Lanzhou 73000, China

10 <sup>2</sup>International Centre for Integrated Mountain Development (ICIMOD), G.P.O. Box 3226, Kathmandu, Nepal

11 <sup>3</sup>Reading Academy, Nanjing University of Information Sciences and Technology 219 Ningliu Road, Nanjing,  
12 Jiangsu, 210044 China.

13 <sup>4</sup>University of Chinese Academy of Sciences, Beijing, China

14 <sup>5</sup>Department of Atmospheric Sciences, Texas A&M University, College Station, TX 77843, USA

15 <sup>6</sup>Research Applications Laboratory, National Center for Atmospheric Research, Boulder, CO 80301, USA

16

17

18

19

20 Correspondence: Siva Praveen Puppala ([sivapraveen.puppala@icimod.org](mailto:sivapraveen.puppala@icimod.org));

21

22

23 **Abstract.** We collected surface snow samples from three different glaciers: Yala, Thana, and Sachin in the central  
24 and western Himalayas to understand the spatial variability and radiative impacts of light-absorbing particles. The  
25 Yala and Thana glaciers in Nepal and Bhutan, respectively, were selected to represent the central Himalayas. The  
26 Sachin glacier in Pakistan was selected to represent the western Himalayas. The samples were collected during the  
27 pre-and post-monsoon seasons of the year 2016. The samples were analysed for black carbon (BC) and water-  
28 insoluble organic carbon (OC) through the thermal optical method. The average mass concentrations (BC ~~2381.39~~  
29  $\text{ng g}^{-1}$ ; OC ~~3896.00~~  $\text{ng g}^{-1}$ ; dust ~~101.95~~  $\mu\text{g g}^{-1}$ ) in the western Himalaya (Sachin glacier) were quite **higher** compared  
30 to the mass concentrations (BC ~~357.938~~  $\text{ng g}^{-1}$ , OC ~~903.864~~  $\text{ng g}^{-1}$ , dust ~~21.952~~  $\mu\text{g g}^{-1}$ ) at the central Himalaya (Yala  
31 glacier). The difference in mass concentration may be due to the difference in elevation, snow age, local pollution  
32 sources, and difference in meteorological conditions. BC in surface snow was also estimated through WRF-Chem  
33 simulations at the three glacier sites during the sampling periods. Simulations reasonably capture the spatial and  
34 seasonal patterns of the observed BC in snow but with a relatively smaller magnitude. Absolute snow albedo was  
35 estimated through the Snow, Ice, and Aerosol Radiation (SNICAR) model. The absolute snow albedo reduction was  
36 ranging **between-from** 0.48 % (Thana glacier during September) to 24 % (Sachin glacier during May) due to BC and  
37 0.13 % (Yala glacier during September) to 5% (Sachin glacier during May) due to dust. The instantaneous radiative  
38 forcing due to BC and dust was estimated in the range of 0 to 96.48  $\text{W m}^{-2}$  and 0 to 25  $\text{W m}^{-2}$  respectively. The  
39 lowest and highest albedo reduction and radiative forcing were observed in central and western Himalayan glaciers,  
40 respectively. The potential source regions of the deposited pollutants were inferred using WRF-Chem tagged-tracer  
41 simulations. Selected glaciers in the western Himalayas were mostly affected by long-range transport from the  
42 Middle East and Central Asia; however, the central Himalayan glaciers were mainly affected by local and South  
43 Asia emissions (from Nepal, India, and China) especially during the pre-monsoon season. Overall, South Asia and  
44 West Asia were the main contributing source regions of pollutants.

45  
46  
47  
48

**Keywords:** black carbon; organic carbon; Yala glacier; Thana glacier; Sachin glacier; snow albedo

## 49 1 Introduction

50 Black carbon (BC) is a distinct type of carbonaceous material that is formed primarily in flames. BC particles in the  
51 atmosphere are generally produced by the incomplete combustion of fossil fuel, biofuel, and biomass. BC is only a  
52 minor contributor to aerosol mass but has a great climatic interest as a strong absorber of solar radiation (Quinn et  
53 al., 2008; Ramanathan and Carmichael, 2008). In addition to warming, BC particles can interact with clouds,  
54 changing their microphysical properties, and thus impacting the climate (Wang et al., 2018; Bond et al., 2013; Dong  
55 et al., 2021). Besides this, several studies in the past highlighted the role of BC on the cryosphere (Kang et al., 2019,  
56 2020).

57  
58 The cryosphere is one of the most sensitive indicators of climate change. The temperature rise in cryospheric regions  
59 is generally larger than that in other regions on the global scale (Pepin and Lundquist 2008; Kang et al., 2010; You  
60 et al., 2021; Huang et al., 2019). BC particles deposit on the glaciers or snow cover surface, decreasing the surface  
61 albedo and absorbing more solar radiation (Warren and Brandt, 2008; He et al., 2017) which accelerates snow and  
62 ice melt and ~~triggering triggers~~ albedo feedback (Flanner et al., 2009; Hansen and Nazarenko, 2004; Kang et  
63 al.,2020). The forcing produced by BC and other light-absorbing particles (LAPs) further affects the regional  
64 climate (Flanner et al., 2009; Xu et al., 2016; Ji et al., 2015) leads to complex responses of the Earth's climate  
65 system (Hansen et al., 1997). The largest climate forcing from BC in the snow is estimated to occur over the Tibetan  
66 Plateau (TP) and Himalayas (Flanner et al., 2009; Ji et al., 2015).

67  
68 Mountain glaciers are the most important freshwater resources to the ~~lives inhabitants~~ of arid and semi-arid regions  
69 (Hock, 2005, 19; Mayer et al., 2006). The ~~great~~-Himalayas is considered as world's largest freshwater reservoir  
70 outside the Polar Regions (Immerzeel et al., 2010; Marcovecchio et al., 2021). The economy and lives of millions of  
71 people in the region are influenced by the changes in mountain river discharge downstream of the Himalayas (Vaux  
72 et al., 2012). Lack of in-situ data, the low resolution of emission inventory, and coarse model resolutions prevent an  
73 accurate evaluation of LAPs impacts on snow albedo and radiative forcing. Many glaciers have retreated in the  
74 region due to climate warming (Zhang et al., 2009; Kang et al., 2010; Yao et al., 2019), and possibly due to LAP-  
75 induced surface darkening (Flanner et al., 2009; Qian et al., 2011; Kang et al., 2019). Glacier retreat in the TP and  
76 the Himalayan region has serious consequences because snow and runoff from this region are sources of major  
77 rivers in Asia, and the availability of freshwater resources has profound effects on human health and agriculture  
78 (Immerzeel et al., 2010). However, ~~it is still~~ large uncertainties ~~remain regarding for~~ glacier retreat driven  
79 predominately by the deposition of BC and other LAPs (Bolch et al., 2012; Kang et al., 2020).

80  
81 Snow albedo is an important indicator of surface energy budget over the snow-covered area. Small changes in  
82 surface snow albedo can have large impacts on surface warming due to the rapid feedbacks involving changes to  
83 sublimation, snow morphology, and melt rates (Bond et al., 2013). The concentration of LAPs in surface snow is a  
84 major factor that affects snow albedo. BC and other LAPs present in the snow reduce the albedo in the visible  
85 portion of the electromagnetic spectrum (e.g., Warren and Wiscombe, 1980, Flanner et al., 2007). Besides the

86 concentration of pollutants deposited on the surface of the snow, multiple other factors, such as solar zenith angle  
87 (SZA), snow grain size, snow **grain** shape, snow **surface** texture, snow density, and snowpack thickness, can also  
88 affect snow albedo (He and Flanner, 2020). The radiative transfer model used for the albedo has brought a better  
89 understanding of snow optical properties in the shortwave spectrum (He and Flanner, 2020). We estimated the  
90 spectral snow albedo using the online Snow, Ice, and Aerosol Radiative (SNICAR) model (Flanner and Zender,  
91 2006). The model was originally developed by Flanner et al., 2007, further updated by He et al. (2018) and Dang et  
92 al., (2019), and has been widely used in simulating the impacts of LAPs on snow albedos (Qu et al., 2014).

93  
94 Here we present the mass concentration of BC, water-insoluble organic carbon (OC), and mineral dust in surface  
95 snow from the ablation and accumulation zones of selected glaciers, located in three different countries (Nepal,  
96 Bhutan, and Pakistan) on the southern slope of the Himalaya. The Yala and Thana glaciers were selected from the  
97 central Himalayas, while the Sachin glacier was selected from the western Himalayas. To reasonably compare the  
98 results (mass concentrations, and optical and radiative properties) across the central and western Himalayas, samples  
99 were collected on similar dates of the same seasons (pre-monsoon and post-monsoon). We investigate the spatial  
100 variability of BC, OC, and mineral dust concentrations due to differences in the source region, meteorology,  
101 deposition, and post-deposition processes. The measured mass concentrations were compared to regional model  
102 simulations. The associated changes in surface snow albedo and radiative forcing (RF) by mineral dust and BC in  
103 surface snow were estimated using the SNICAR model. We also aim to identify the potential source regions of  
104 pollution reaching sampling sites using tracer-tagged model simulations.

## 105 106 **2 Study area and meteorology**

107 Samples were collected from the Yala glacier (28°14' N, 85°37' E) in the Langtang valley of Nepal, the Thana  
108 glacier (28°01' N, 90°36' E) in the Chamkhar valley of Bhutan, and the Sachin glacier (35°19' N, 74°45' E) in  
109 northern Pakistan (Table 1). Monthly mean surface air temperature and precipitation (MERRA-2 reanalysis data)  
110 over the selected glaciers were analyzed and compared for the western and central Himalayan glaciers from April  
111 2015 to October 2017 (Table 2). Yala Glacier is a plateau-shaped glacier that has an elevation range between 5160  
112 and 5750 m a.s.l. The length of the Yala glacier is 1.5 km facing the northwest. The glacier is located away from the  
113 residential area and is mostly covered by **firm**/**firn**/snow, especially during the winter season. Details about the  
114 metrological condition at the Yala glacier are available in Mukesh et al., (2019) and Gul et al., (2021). Thana glacier  
115 is a gentle slope glacier with slight debris cover and an elevation range between 5250 and 5700 m a.s.l. The length  
116 of the glacier is about 5 km, facing the southwest. The Thana glacier is mostly covered by fresh snow especially  
117 during the winter season. The Sachin glacier has a gentle slope with dense debris cover in its ablation area with an  
118 altitude range from 3105 to 4976 m a.s.l. The length of the Sachin glacier is around 8 km facing northeast. In  
119 general, the **Sachin-glacier is a low elevated-elevation and** relatively debris-covered **glaciers as-c** compared to **the**  
120 **central** Himalayan glaciers (Yala and Thana). Precipitation in central Himalayan glaciers (Yala and Thana) was  
121 higher than that of the western Himalayan glacier (Sachin) especially from April to October each year (Table 2).  
122 Surface air temperature over the Yala and Sachin glacier was higher than that of the Thana glacier. The geographical

123 location of the selected glaciers and snow sampling locations are shown in Fig. 1. Besides the difference in altitude,  
124 latitude, and meteorology of the selected glaciers in the central and western Himalayas, there is also a difference in  
125 the surface condition shown in supplementary Fig. S1.

126

### 127 3 Methodologies

128

#### 129 3.1 Snow sampling and analysis

130 ~~Surface Snow-snow~~ samples were collected from the central and western Himalayan glaciers during May, and  
131 September 2016. Samples were taken ~~from the surface of the~~ **from the ablation and accumulation zones of the**  
132 selected glaciers; however, **a few snow samples were also collected from the surrounding nearby areas of the Yala**  
133 **and Sachin glaciers. Sachin glacier's samples were relatively aged snow and had less snow thickness as compared to**  
134 **the samples collected from Thana and Yala glaciers (supplementary Fig. S1). At each sampling location, Whirl-Pak**  
135 **bags were used to collect samples from the upper 0-10 cm of depth (approximately 2 L, unmelted). The samples**  
136 **were kept frozen until they were melted and filtered in through the quartz filters near the sampling site.** The snow  
137 density was measured with a small density kit. The snow grain size was measured through a hand lens (25×) with an  
138 accuracy of 0.02mm. **The same sampling protocol was used for all the three selected glaciers.** A detailed description  
139 of the sampling procedure is described in **Gul-Li et al.,-2021+2016a**. Quartz filters were used to measure the mass  
140 concentration of BC, OC, and dust in the collected samples. BC and OC present in snow samples were analyzed by a  
141 filter-based thermal-optical analysis method using DRI® Model 2005 (Chow et al., 1993). Filters were analyzed at  
142 the State Key Laboratory of Cryosphere Science, Northwest Institute of Eco-Environment and Resources, Chinese  
143 Academy of Sciences. Before starting the analysis, a piece of the sampled filters was put in an oven for a few  
144 minutes to eliminate the water vapor content and volatile organic compounds. Further detailed information on the  
145 instrument and analysis method can be referred to in earlier studies (Gul et al., 2018, **2021**).

146

#### 147 3.2 Estimation of snow albedo reduction and radiative forcing

148 The online snow simulation model SNICAR (Flanner et al., 2007, <http://snow.engin.umich.edu/>) was used to  
149 estimate snow albedo calculation for the collected samples. The model has been used by multiple studies in the past  
150 (e.g., Li et al., 2017; Gul et al., 2018; Zhang et al., 2018 ). Albedo was simulated based on an hourly SZA at the  
151 sampling site with an averaged mass concentration of BC, dust, and other input parameters such as snow grain size,  
152 snow density, and snow depth from measurements. We computed broadband snow albedo for direct solar incident  
153 radiation under the mid-latitude winter clear sky condition, (Supplementary Table S1). Depending on geographical  
154 location, 10 to 15 SZAs were used (between 0° and 90°) during instantaneous daytime albedo simulation. Albedo  
155 was simulated in four categories: 1- broadband albedo with BC and dust in snow, 2- broadband albedo with BC in  
156 snow only, 3- broadband albedo with dust in snow only, and 4- broadband albedo with the absence of BC and dust  
157 which was considered as a reference albedo. Radiative implications caused by snow darkening due to BC and dust  
158 deposition were investigated using the albedo reduction and the radiative transfer model Santa Barbara DISORT  
159 Atmospheric Radiative Transfer (SBDART) (Ricchiuzzi et al., 1998). To evaluate the amount of additional solar

160 radiations absorbed by the snow in the presence of BC and dust, we estimated the mean solar irradiance and its  
161 characteristics via SBDART, which has been used in the past (Yang et al., 2015). According to the location of the  
162 sampling site, the characteristics of the atmospheric profiles such as water vapor, aerosols, ozone, etc. were set in the  
163 model. ~~RF based on measured BC and dust concentration in our samples were estimated using the following~~  
164 ~~equation. RF for the snow samples was estimated by following Eq. (1):~~

$$165 \quad RF_x = R_{in-short} * \Delta \alpha_x \quad (1)$$

166 where,  $R_{in-short}$  denotes incident short-wave solar radiation for selected SZA and  $\Delta\alpha_x$  denotes the reduction in albedo  
167 due to BC, dust, or both, as simulated by the SNICAR model.

168

### 169 3.3 Potential source region of pollutants

170 Glaciers of the Himalaya Karakoram and Hindukush (HKH) region are located at high altitudes as compared to the  
171 sources of the major pollutants. LAPs including BC and dust can transport from urban areas towards glaciated areas  
172 (e.g., Yasunari et al., 2009; Kang et al., 2019). Multiple approaches, including climate circulation modeling,  
173 combinations of bottom-up inventories, and back air trajectories have been used in the past to determine the possible  
174 source regions of pollution in the HKH region. To identify the potential source region of pollution arriving at the  
175 observation sites, we used ~~for the central and western Himalayan glaciers,~~ the weather research and forecasting  
176 (WRF) model coupled with chemistry (WRF-Chem version 3.9.1.1) simulations (Grell et al., 2005). ~~The model uses~~  
177 ~~region-tagged-tracers simulations for the selected sites for different regions across the world.~~

178

179 WRF-Chem simulations were used to estimate BC mass concentration in surface snow and deposition of BC  
180 particles on three selected glaciers (Yala, Thana, and Sachin). We archived the hourly model results for  
181 instantaneous BC deposition and concentration in snow. The horizontal grid spacing of the model was 20 km x 20  
182 km with 35 vertical levels stretching from the surface up to 50 hPa (~20 km). The updated Model for Ozone And  
183 Related chemical Tracers (MOZART) was applied for the gas phase chemistry (Knote et al., 2014) while aerosols in  
184 the WRF-Chem were simulated via the Model for Simulating Aerosol Interactions and Chemistry (MOSAIC)  
185 (Zaveri et al., 2008). We use the Global Data Assimilation System (GDAS) from the National Center for  
186 Environmental Prediction (NCEP) for the meteorological initial and boundary conditions. We used the Fire  
187 Inventory from NCAR (FINN), the EDGAR-HTAP, and MEGAN (Model of Emissions of Gases and Aerosols from  
188 Nature) for biomass burning emissions, anthropogenic emissions, and ~~for online~~ biogenic emissions, respectively.  
189 For chemical boundary conditions, we used the NCAR global CAM-Chem simulation dataset  
190 (<https://rda.ucar.edu/datasets/ds313.7/>). Key meteorological variables such as winds, temperature, and water vapor  
191 above the planetary boundary layer (PBL) were nudged every 6 hours towards the NCEP GDAS reanalysis fields to  
192 reduce temporal error growth in meteorological variables. We used the Community Land Model (CLM) scheme for  
193 the land component in WRF-Chem. The CLM model can simulate BC concentration in snowpack and its effects on  
194 snow albedo (Flanner et al., 2007). We used online coupled BC deposition fluxes from the atmosphere component  
195 of WRF-Chem with the CLM model following Zhao et al. (2014). We also implemented a tagged-tracer method  
196 (Kumar et al., 2015) to track anthropogenic BC emissions from 10 different Asian countries surrounding the TP

197 areas, as well as BC emissions from Asian biomass burning and the domain boundary (i.e., areas outside Asia). The  
198 tracked 10 anthropogenic emission source regions include China, India, Nepal, Pakistan, Afghanistan, Bhutan,  
199 Bangladesh, Myanmar, Southeast Asia, and the rest of Asia. The aim of the model simulation was to estimate the  
200 BC mass concentration in surface snow, deposition of BC particles, and the source contribution to BC deposition on  
201 snow.

202

## 203 4. Results and discussions

### 204 4.1 Concentrations of light-absorbing particles in surface snow

205 The average mass concentration of LAPs in surface snow of the Yala glacier was 357.938 ng g<sup>-1</sup> for BC, 903.864 ng  
206 g<sup>-1</sup> for OC, and 24.952 µg g<sup>-1</sup> for dust in spring (May) and was relatively lower concentrations of 68.979 ng g<sup>-1</sup> for  
207 BC, 177.50 ng g<sup>-1</sup> for OC and 4.3 ng g<sup>-1</sup> for dust during autumn (September). These mass concentrations of BC and  
208 OC in surface snow were comparable to the study result conducted on the Yala glacier in May 2017 (Gul et al.,  
209 2021).

210 High LAP concentration in the pre-monsoon is due to an effective transport mechanism from seasonally high the  
211 Indian subcontinent emission (Kang et al., 2019; Gul et al., 2021) and an additional source such as forest fires (Gul  
212 et al., 2021). Lau et al., (2010) also confirmed that aerosols from biofuel and biomass burning rapidly build up  
213 over Indo-Gangetic Plains (IGP) and East Asia during pre-monsoon season and move towards the study site. The  
214 average surface concentrations of BC, OC, and dust in the Thana glacier samples during the autumn season were  
215 39.39 ng g<sup>-1</sup>, 115ng g<sup>-1</sup> and 34.63 µg g<sup>-1</sup>, respectively. Possible reasons for the lowest lower concentration at the  
216 Thana glacier may be due to the relatively high elevation of the sampling location and relatively fresh snow. A  
217 strong effect of LAPs (BC and dust) has been observed at lower elevations in comparison to higher elevations (Li et  
218 al., 2017). The average concentration of BC, OC, and dust measured in the selected western Himalayan glacier  
219 (Sachin) during May were 2381.39 ng g<sup>-1</sup>, 3896 ng g<sup>-1</sup> and 101 µg g<sup>-1</sup>, respectively, and were relatively higher  
220 during October with values of 5314 ng g<sup>-1</sup> for BC, and 546 µg g<sup>-1</sup> for dust (Gul et al., 2018). The observed average  
221 mass concentrations in the western Himalayas were higher than those in the central Himalayas. The BC mass  
222 concentration difference might be due to the difference in snow type, precipitation rate, local emission, the elevation  
223 of sampling sites, meteorology, and BC deposition over the glacier surfaces. Post dry deposition of LAPs over the  
224 surface of the snow was an important factor. The pollutants source regions for the central and western Himalayas are  
225 different. In the case of central Himalayas, pollutants emitted during pre-monsoon convection and multiple forest  
226 fires events are effectively lifting and transported towards central Himalayan glaciers. Due to strong inversion in  
227 winter, most of the pollutants get stuck near-surface whereas in monsoon pollutants get scavenged by rain. Thus pre-  
228 monsoon is a very significant period in the transport process in the central Himalayas. Snow samples collected from  
229 the western side of the Himalayas were aged as compared to the central side; post-deposition ion (or enrichment) of  
230 LAPs over the snow surface increased the concentration in the snow (Kang et al., 2019). The majority of the  
231 samples from the western Himalayan side were from ablation zones of the glacier, where concentrations of LAPs are  
232 higher as compared to the accumulation zone of the glacier. Li et al., (2017) showed a strong negative relationship  
233 between the elevation of glacier sampling locations and the concentration of LAPs. Therefore strong melting of

Formatted: Adjust space between Latin and Asian text, Adjust space between Asian text and numbers

Formatted: Highlight

234 surface snow and ice in the glacier ablation zone could lead to BC enrichment which causes high BC concentrations  
235 (Li et al., 2017). In the case of western Himalayan glaciers sites, snow samples were collected long after the  
236 snowfall and the concentration of pollutants would also have increased in the surface snow due to dry deposition.  
237 The surface concentrations of the individual samples collected from the Yala, Thana, and Sachin glaciers during  
238 May and September 2016 are shown in Fig. 2, and Table S2. BC and OC concentration on our selected glaciers with  
239 a comparison to other glaciers of TP and the surrounding region are shown in Fig. 4-3 and Table S3. It was observed  
240 that the concentration of BC, OC, and dust in the central Himalayan glaciers (Yala and Thana) were comparable to  
241 other reported results. In the past, similarly high concentrations were reported in the region (Xu et al., 2012) such as  
242 Tien Shan Mountains (Li et al., 2016), Northeast of the TP (Wang et al., 2016), Northern China (Zhang et al., 2016)  
243 Southeastern TP, western Tien Shan and Central Asia (Zhang et al., 2017). ▲

Formatted: Highlight

Formatted: Font color: Auto

244  
245 The yellow boxes of Fig. 2 show the WRF-Chem modeled BC concentrations in surface snow at the three  
246 measurement glacier sites during the measurement periods. Compared to the observations red boxes in Fig. 2, model  
247 results reasonably capture the spatial and seasonal patterns and variables of the observed BC in the snow with a  
248 relatively smaller magnitude. The modeled variation at the Sachin site during the October sampling periods is much  
249 larger than the observations (Gul et al., 2018). The discrepancies between model results and observations are due to  
250 model uncertainties from (1) the relatively coarse grid spacing that may not capture the transport over the complex  
251 TP terrain, (2) the underestimated anthropogenic emissions that are not representative ~~for-of~~ the measurement  
252 periods, and (3) deficiencies in model physical parameterizations that affects BC transport and deposition. **The**  
253 **WRF-Chem model implicitly accounts for the surface impurity enrichment during snow ablation by using a low**  
254 **meltwater scavenging efficiency for BC. However, we notice that this meltwater scavenging efficiency parameter**  
255 **could be associated with large uncertainties (Qian et al., 2014) due to the lack of direct observational constraints.** We  
256 also note that the observed variation at each site shown in Fig. 2 includes both the temporal and subgrid variabilities  
257 derived from multiple sampling locations surrounding each site (Fig. 1). In contrast, all the measurement locations at  
258 each particular glacier site are located within a single model grid. As a result, the model is unable to resolve this  
259 subgrid information and hence only includes the temporal variability for each selected site.

#### 261 4.2 Surface snow albedo and radiative forcing

262 The minimum daytimes absolute albedo reduction due to combined BC and dust, BC only and dust only were in the  
263 range (1.03-13.44%), (0.48-12.42%) and (0.12-2.12%), respectively. The maximum daytime albedo reduction due to  
264 combined BC and dust, BC only and dust only was in the range (1.98-24.97%), (1.05-24%), and (0.25-4.8%)  
265 respectively. The lowest and highest contributions in albedo reduction were observed in the central Himalayas  
266 (September) and the western Himalayas (May) respectively. Snow albedo reduction (%) derived from samples  
267 collected from the Yala glacier (during May 2016) and the Thana glacier (during September 2016) were in the range  
268 of (0.13-3.82%) and (0.90-1.99%), respectively. A significant difference in daytime albedo reduction between the  
269 western and central Himalayas was mainly due to the difference in mass concentrations of pollutants and snow age.  
270 The pollutant concentrations in the western Himalayan samples (Sachin glacier) were higher, resulting in higher



271 albedo reduction as compared to the central Himalayan (Yala and Thana glaciers) samples. The average elevation  
272 difference between central and western sampling sites was greater than 1000 meters, where a high concentration of  
273 pollution is expected at the low elevated glacier of the western side as compared to the central side of the Himalaya.  
274 Snow samples collected on the central side of the Himalayas (Yala glacier) were much fresher as compared to the  
275 samples collected from the western side (Sachin glacier). Dust and other pollutants were visible over the surface of  
276 the Sachin glacier (Fig. S1). Aged snow had increased density, enlarged grain size, and increased concentration of  
277 BC and dust particles due to dry deposition on the snow surface. In the case of all sampling sites impact of BC on  
278 snow albedo reduction was greater than the impact of dust except the Thana glacier where the impact of dust was  
279 higher than that of BC (Fig. 4a). This may be due to a different dust type in Thana samples. Daytime snow albedo  
280 reductions (%) due to BC only, dust only, and both BC and dust are given in Fig. 4a.

281  
282 The daytime instantaneous RF ( $W m^{-2}$ ) ranged from (0.076 to 39.65) for the Yala glacier during-in May 2016, 0.006  
283 to 18.26 for the Yala glacier during-in September 2016, 0.0 to 11.48 for the Thana glacier during-in September 2016,  
284 and 0.03 to 96.48 for the Sachin glacier during May 2016. RF for the western Himalayas (Sachin glacier) was quite  
285 high as compared to the central Himalayan glaciers (Yala and Thana glaciers). The radiative effect on the Sachin  
286 glacier was much more than that of other selected glaciers mainly due to low albedo and increased temperature.  
287 Zhang et al. (2017) reported that a reduction in albedo by 9 to 64 % can increase the instantaneous RF by as much as  
288 24.05–323.18  $W m^{-2}$ . In the case of all sampling sites impact of BC on RF was greater than the impact of dust  
289 except the Thana glacier where the impact of dust was higher than that of BC (Fig. 4b). Therefore, BC can be a  
290 major responsible pollutant in the snow to reduce albedo and increase warming in the selected glaciers. BC was the  
291 dominant factor in snow melting in the Yala and Sachin glaciers; however, dust was the dominant factor in Thana  
292 glacier samples. According to (Kaspari et al., 2014), RF caused by mineral dust was greater than that of dust. The  
293 BC and dust had low importance for RF in fresh snow (central Himalaya - Thana glacier) as compared to aged snow  
294 (western Himalaya - Sachin glacier). In the northern TP, BC played important role in RF (Li et al., 2016a), while in  
295 the central TP and Himalayas dust was more important than BC (Kaspari et al., 2014). The average instantaneous  
296 RF caused by the combined contribution of BC and dust (BC + dust), only BC, and only dust is shown in Fig. 4b as  
297 a function of surface snow types. Variation in the RF and albedo change for a particular pollutant type was due to  
298 variation in SZA.

299

### 300 **5 Potential source regions of pollutants**

301 Figure 5 shows the contributions of different BC emission sources to the BC in snow from WRF-Chem tagged-  
302 tracer simulations. For the Yala site, it is dominated (>50%) by anthropogenic emissions from India and Nepal for  
303 both May and October, while the biomass burning contribution (>20%) increases largely in May primarily due to the  
304 spring burning activities in northern India (Kumar et al., 2011). In September, China's contribution also increases to  
305 >20% at Yala. For the Thana site, it is dominated (>60%) by anthropogenic emissions from China and India in  
306 September, while anthropogenic emissions from Bhutan and Myanmar also contribute about 10%, respectively. The  
307 Sachin site is predominantly affected by anthropogenic emissions from India and Pakistan (total contribution

308 >80%), while the spring biomass burning only contributes to ~10% in May. Overall, the source contributions show  
309 large variation depending on the site locations and sampling seasons, but with a consistent India contribution of 20-  
310 40% across all the sites and seasons.

311

## 312 **6 Discussion on uncertainty in measurements, albedo, and potential source identification of pollutants**

313 The possible uncertainties in the present research were related to measurements, sampling, analysis, albedo, and RF  
314 estimation. A sampling at remote rural sites, sample preservation, filtration, and transport can modify the results if  
315 proper standard protocols were not followed. During laboratory analysis via thermal optical techniques, several  
316 uncertainties may be related to separating OC from BC in the sample (Gul et al., 2021). The level of generated  
317 uncertainty depended on temperature protocol, sample type (residential cookstoves, diesel exhaust, rural aerosols,  
318 and urban aerosols), the amount of dust loading on the filter, and the analysis method. The overall accuracy in the  
319 measurement of OC, BC, and total carbon concentrations was estimated considering the mass contributions from  
320 field blanks and the analytical accuracy of concentration measurements. The uncertainty of the OC and BC mass  
321 concentrations was extracted through the standard deviation of the field blanks (Li et al., 2021). OC in snow can  
322 produce minor warming (Yasunari et al., 2015), but in this research albedo reduction from OC was not quantified. In  
323 albedo simulation and RF estimations, snow grain size and texture can produce large uncertainty. We  
324 measured/considered the physical grain size in this research which is not the same as the effects than optical grain  
325 size. Optical grain size defines the amount of solar radiation absorbed/scattered by the snow. We assumed a  
326 spherical shape for the snow grains which may affect the results because the albedo of non-spherical grains is higher  
327 than the albedo of spherical grains (Dang et al., 2016; He et al., 2018). The contribution of pollutants generated from  
328 local sources can be important (e.g., Li et al., 2021), which however was not included in the global emission  
329 inventories; we were unable to capture emissions at the local scale. Therefore contributions of local sources may be  
330 underestimated by coarse-resolution models. High-resolution models and emission inventories at the local scale are  
331 required to capture local emissions.

332

## 333 **7 Conclusions**

334 The average mass concentration of LAPs in the samples collected from the Sachin, Yala, and Thana glaciers were in  
335 the range (835.324 ng g<sup>-1</sup> to 3545.35 ng g<sup>-1</sup> for BC and 35.24 µg g<sup>-1</sup> to 253.52 µg g<sup>-1</sup> for Dust), (23.46 ng g<sup>-1</sup> to  
336 2529 ng g<sup>-1</sup> for BC and 1.5 µg g<sup>-1</sup> to 196.5 µg g<sup>-1</sup> for Dust), and (21 ng g<sup>-1</sup> to 127 ng g<sup>-1</sup> for BC and 1.5 µg g<sup>-1</sup> to 67  
337 µg g<sup>-1</sup> for Dust) respectively. Overall the concentrations of BC and dust were varied from 21 ng g<sup>-1</sup> and 1.5 µg g<sup>-1</sup>  
338 fresh snow to 3545 ng g<sup>-1</sup> and 253 µg g<sup>-1</sup> in the aged snow, respectively. Mass concentrations of BC, OC, and dust in  
339 the samples collected from the western Himalayas was much higher than the average concentration in the central  
340 Himalayas mainly due to difference in snow age, elevation, and meteorology. The accumulation area of glaciers  
341 (e.g. ice cores and snow pits), where enrichment influences are less marked and measured values are likely to be  
342 lower, and high elevation areas, where deposition of pollutants is expected to be lower. Pollutant concentrations  
343 were likely underestimated in the earlier studies, particularly when there was strong surface melting. Dust and other  
344 pollutants were visible on aged snow surfaces in the western Himalayan glacier, indicating considerable enrichment

345 during snow aging. WRF-Chem modeled BC concentrations in surface snow were almost similar to the observed BC  
346 in the snow with a relatively smaller magnitude.

347  
348 Based on observed pollutants, snow albedo reduction (%) in the central Himalayas was in the range of (0.48-3.6%  
349 for BC) and (0.13-1.99% for Dust), much lower than that of the western Himalayas. BC was the major component  
350 responsible for the albedo reduction, and the dust had little effect except in the Thana glacier. In case the of the  
351 Thana glacier, the impact of dust was higher than that of BC. The daytime instantaneous radiative forcing ( $W\ m^{-2}$ )  
352 ranged from 0.076 to 39.65 (Yala glacier during May 2016), 0.006 to 18.26 (Yala glacier during September 2016),  
353 0.0 to 11.48 (Thana glacier during September 2016), 0.03 to 96.48 (Sachin glacier during May 2016). The average  
354 albedo reduction due to the combined effect of dust and BC at the western Himalayan side (Sachin glacier) was  
355 0.372 which was~ 15 times higher than that of the central Himalayan side (Yala glacier). Similarly, the radiative  
356 forcing in the western Himalayas ~~was~~ ~~was~~~ 6 times higher than that of the central Himalayan side. Observation  
357 showed that the potential source regions of pollutants for the western and central Himalayas were different. Western  
358 Himalayan glaciers were mostly affected by long-range transport via the westerlies; however central Himalayan  
359 glaciers were affected by relatively local winds from Nepal, Bhutan, India, and China. For the western Himalayan  
360 glaciers, the emissions from central Asian and South Asian countries (Particularly Pakistan and India) are more  
361 important source regions.

362

### 363 **Acknowledgment**

364 This study was supported by the National Natural Science Foundation of China (41630754), the Chinese Academy  
365 of Sciences (XDA20040501, QYZDJ-SSW-DQC039), and the State Key Laboratory of Cryosphere Science  
366 (SKLCS-ZZ-2021). This study was also partially supported by the core funds of ICIMOD contributed by the  
367 governments Afghanistan, Australia, Austria, Bangladesh, Bhutan, China, India, Myanmar, Nepal, Norway,  
368 Pakistan, Sweden, and Switzerland. We thank Faiza Gul, Aditi Mukherji, and Arnico Panday for their useful  
369 comments and guidance. We are also grateful to the staff of the National Centre for Hydrology and Meteorology in  
370 Bhutan for organizing the Thana Glacier expedition in 2016. We would like to acknowledge high-performance  
371 computing support from Cheyenne provided by NCAR's Computational and Information Systems Laboratory,  
372 sponsored by the National Science Foundation. NCAR is operated by the University Corporation for Atmospheric  
373 Research under the sponsorship of the National Science Foundation.

374

### 375 **References**

376 Bolch, T., Kulkarni, A., Kääb, A., Huggel, C., Paul, F., Cogley, J. G., Frey, H., Kargel, J. S., Fujita, K., Scheel, M.,  
377 Bajracharya, S., and Stoffel, M.: The State and Fate of Himalayan Glaciers, *Science*, 336, 310–314, 2012.  
378 Bond, T. C., Doherty, S. J., Fahey, D. W., Forster, P. M., Berntsen, T., DeAngelo, B. J., Flanner, M. G., Ghan, S.,  
379 Kärcher, B., Koch, D., Kinne, S., Kondo, Y., Quinn, P. K., Sarofim, M. C., Schultz, M. G., Schulz, M.,  
380 Venkataraman, C., Zhang, H., Zhang, S., Bellouin, N., Guttikunda, S. K., Hopke, P. K., Jacobson, M. Z., Kaiser,

381 J. W., Klimont, Z., Lohmann, U., Schwarz, J. P., Shindell, D., Storelvmo, T., Warren, S. G., and Zender, C. S.:  
382 Bounding the role of black carbon in the climate system: A scientific assessment, *J. Geophys. Res.-Atmos.*, 118,  
383 5380–5552, doi:10.1002/jgrd.50171, 2013.

384 Chow, J. C., Watson, J. G., Pritchett, L. C., Pierson, W. R., Frazier, C. A., and Purcell, R. G.: The DRI  
385 thermal/optical reflectance carbon analysis system: description, evaluation, and applications in US air quality  
386 studies, *Atmos. Environ. A-Gen.*, 27, 1185–1201, 1993.

387 Dang, C., Zender, C. S., and Flanner, M. G. (2019), Intercomparison and improvement of twostream shortwave  
388 radiative transfer schemes in Earth system models for a unified treatment of cryospheric surfaces, *The*  
389 *Cryosphere*, 13, 2325–2343, doi:10.5194/tc-13-2325-2019, 2019.

390 Dang, C., Fu, Q., and Warren, S. G.: Effect of snow grain shape on snow albedo, *J. Atmos. Sci.*, 73, 3573–  
391 3583, <https://doi.org/10.1175/JAS-D-15-0276.1>, 2016.

392 Flanner, M. G. and Zender, C. S.: Linking snowpack microphysics and albedo evolution, *J. Geophys. Res. Atmos.*,  
393 111(12), 1–12, doi:10.1029/2005JD006834, 2006.

394 Flanner, M. G., Zender, C. S., Randerson, J. T. and Rasch, P. J.: Present-day climate forcing and response from black  
395 carbon in snow, *J. Geophys. Res. Atmos.*, 112(11), 1–17, doi:10.1029/2006JD008003, 2007.

396 Flanner, M. G., Zender, C. S., Hess, P. G., Mahowald, N. M., Painter, T. H., Ramanathan, V. and Rasch, P. J.:  
397 Springtime warming and reduced snow cover from carbonaceous particles, *Atmos. Chem. Phys. Discuss.*, 8(6),  
398 19819–19859, doi:10.5194/acpd-8-19819-2008, 2009.

399 Grell, G. A., Peckham, S. E., Schmitz, R., McKeen, S. A., Frost, G., Skamarock, W. C., and Eder, B.: Fully coupled  
400 “online” chemistry within the WRF model, *Atmos. Environ.*, 39, 6957–6975, 2005.

401 Gul, C., Puppala, S.P., Kang, S., Adhikary, B., Zhang, Y., Ali, S., Li, Y., Li, X., 2018. Concentrations and source  
402 regions of light-absorbing particles in snow/ice in northern Pakistan and their impact on snow albedo. *Atmos.*  
403 *Chem. Phys.* 18, 4981–5000. <https://doi.org/10.5194/acp-18-4981-2018>

404 Gul, C., Mahapatra, P.S., Kang, S., Singh, P.K., Wu, X., He, C., Kumar, R., Rai, M., Xu, Y., Puppala, S.P., Black  
405 carbon concentration in the central Himalayas: impact on glacier melt and potential source contribution,  
406 *Environmental Pollution*, <https://doi.org/10.1016/j.envpol.2021.116544>, 2021

407 Hansen, J. and Nazarenko, L.: Soot climate forcing via snow and ice albedos, *Proc. Natl. Acad. Sci. U. S. A.*, 101(2),  
408 423–428, doi:10.1073/pnas.2237157100, 2004.

409 Hansen, J., Sato, M. & Ruedy, R.: Radiative forcing and climate response, *J. Geophys. Res.* 102, 6831–6864,  
410 doi.org/10.1029/96JD03436, 1997

411 He, C., Flanner, M. G., Chen, F., Barlage, M., Liou, K.-N., Kang, S., Ming, J., and Qian, Y.: Black carbon-induced  
412 snow albedo reduction over the Tibetan Plateau: uncertainties from snow grain shape and aerosol–snow mixing  
413 state based on an updated SNICAR model, *Atmos. Chem. Phys.*, 18, 11507–11527, <https://doi.org/10.5194/acp-18-11507-2018>, 2018

414 He, C., & Flanner, M. (2020). Snow Albedo and Radiative Transfer: Theory, Modeling, and  
415 Parameterization. Kokhanovsky A, editor, 67-133.

416 He, C., Takano, Y., Liou, K. N., Yang, P., Li, Q., & Chen, F. (2017). Impact of snow grain shape and black carbon–

418 snow internal mixing on snow optical properties: Parameterizations for climate models. *Journal of*  
419 *Climate*, 30(24), 10019-10036. doi:10.1175/JCLI-D-17-0300.1

420 Hock R.: Glacier melt: a review of processes and their modelling. *Progr. Phys. Geogr.*, 29(3), 362–391, doi:  
421 10.1191/0309133305pp453ra, 2005.

422 Hock, R., G. Rasul, C. Adler, B. Cáceres, S. Gruber, Y. Hirabayashi, M. Jackson, A. Kääb, S. Kang, S. Kutuzov, Al.  
423 Milner, U. Molau, S. Morin, B. Orlove, and H. Steltzer, 2019: High Mountain Areas. In: *IPCC Special Report on*  
424 *the Ocean and Cryosphere in a Changing Climate* [H.-O. Pörtner, D.C. Roberts, V. Masson-Delmotte, P. Zhai,  
425 M. Tignor, E. Poloczanska, K. Mintenbeck, A. Alegria, M. Nicolai, A. Okem, J. Petzold, B. Rama, N.M. Weyer  
426 (eds.)]. In press.

427 Immerzeel, W. W., van Beek, L. P. H. and Bierkens, M. F. P.: Climate change will affect the Asian water towers.,  
428 *Science*, 328(5984), 1382–5, doi:10.1126/science.1183188, 2010.

429 Ji Z., S. Kang, Z. Cong, Q. Zhang, T. Yao. 2015. Simulation of carbonaceous aerosols over the Third Pole and  
430 adjacent regions: distribution, transportation, deposition, and climatic effects. *Climate Dynamics*, 45(9-10):  
431 2831-2846. <https://doi.org/10.1007/s00382-015-2509-1>.

432 Kang S., Y. Zhang, Y. Qian, H. Wang. 2020. A review of black carbon in snow and ice and its impacts on  
433 cryospheric change. *Earth-Science Reviews*, 210, 103346. <https://doi.org/10.1016/j.earscirev.2020.103346>.

434 Kang S., Q. Zhang, Y. Qian, Z. Ji, C. Li, Z. Cong, Y. Zhang, J. Guo, W. Du, J. Huang, Q. You, A. K. Panday, M.  
435 Rupakheti, D. Chen, Örjan Gustafsson, M. H. Thiemens, D. Qin. 2019. Linking Atmospheric Pollution to  
436 Cryospheric Change in the Third Pole Region: Current Progresses and Future Prospects. *National Science*  
437 *Review*, 6(4): 796-809. <https://doi.org/10.1093/nsr/nwz031>.

438 Kang S., X. Wei, Q. You, Wolfgang-Albert Flügel, Nick Pepin, T. Yao. 2010. Review of climate and cryospheric  
439 change in the Tibetan Plateau. *Environmental Research Letter*, 5(2010) 015101 (8pp).  
440 <https://doi.org/10.1088/1748-9326/5/1/015101>.

441 Kaspari, S., Painter, T. H., Gysel, M., Skiles, S. M. and Schwikowski, M.: Seasonal and elevational variations of  
442 black carbon and dust in snow and ice in the Solu-Khumbu, Nepal and estimated radiative forcings, *Atmos.*  
443 *Chem. Phys.*, 14(15), 8089–8103, doi:10.5194/acp-14-8089-2014, 2014.

444 Knote, C., Hodzic, A., Jimenez, J. L., Volkamer, R., Orlando, J. J., Baidar, S., Brioude, J., Fast, J., Gentner, D. R.,  
445 Goldstein, A. H., Hayes, P. L., Knighton, W. B., Oetjen, H., Setyan, A., Stark, H., Thalman, R., Tyndall, G.,  
446 Washenfelder, R., Waxman, E., and Zhang, Q.: Simulation of semi-explicit mechanisms of SOA formation from  
447 glyoxal in aerosol in a 3-D model, *Atmos. Chem. Phys.*, 14, 6213–6239, doi:10.5194/acp-14-6213-2014, 2014.

448 Kumar, R., Barth, M. C., Nair, V. S., Pfister, G. G., Suresh Babu, S., Satheesh, S. K., Krishna Moorthy, K.,  
449 Carmichael, G. R., Lu, Z., and Streets, D. G.: Sources of black carbon aerosols in South Asia and surrounding  
450 regions during the Integrated Campaign for Aerosols, Gases and Radiation Budget (ICARB), *Atmos. Chem.*  
451 *Phys.*, 15, 5415-5428, <https://doi.org/10.5194/acp-15-5415-2015>, 2015.

452 Kumar, R., Naja, M., Satheesh, S. K., Ojha, N., Joshi, H., Sarangi, T., Pant, P., Dumka, U. C., Hegde, P.,  
453 and Venkataramani, S. (2011), Influences of the springtime northern Indian biomass burning over the central  
454 Himalayas, *J. Geophys. Res.*, 116, D19302, doi:10.1029/2010JD015509.

455 Lau, K. M., Kim, M. K., and Kim, K. M.: Enhanced surface warming and snow melt in the Himalayas and Tibetan  
456 Plateau induced by the EHP effect, *Environ. Res. Lett.*, *5*, 025204, doi:10.1088/1748-9326/5/2/025204, 2010.

457 Li, C., Bosch, C., Kang, S., Andersson, A., Chen, P., Zhang, Q., Cong, Z., Chen, B., Qin, D., and Gustafsson, Ö.:  
458 Source of black carbon to the Himalayan-Tibetan Plateau glaciers, *Nat. Commun.*, *7*, 12574,  
459 <https://doi.org/10.1038/ncomms12574>, 2016a.

460 Li, C., Yan, F., Kang, S., Yan, C., Hu, Z., Chen, P., ... & Stubbins, A. (2021). Carbonaceous matter in the atmosphere  
461 and glaciers of the Himalayas and the Tibetan plateau: An investigative review. *Environment International*, *146*,  
462 106281

463 Li, X., Kang, S., He, X., Qu, B., Tripathee, L., Jing, Z., Paudyal, R., Li, Y., Zhang, Y., Yan, F., Li, G. and Li, C.:  
464 Light-absorbing impurities accelerate glacier melt in the Central Tibetan Plateau, *Sci. Total Environ.*,  
465 doi:10.1016/j.scitotenv.2017.02.169, 2017.

466 Li, Yang, S. Kang, Xuelei Zhang, Jizu Chen, Julia Schmale, Xiaofei Li, Yulan Zhang, Hewen Niu, Zhongqin Li,  
467 Xiang Qin, Xiaobo He, Wei Yang, Guoshuai Zhang, Shijin Wang, Lili Shao, Lide Tian. 2021. Black carbon and  
468 dust in the Third Pole glaciers: Revaluated concentrations, mass absorption cross-sections and contributions to  
469 glacier ablation. *Science of the Total Environment*, 789: 147746. <https://doi.org/10.1016/j.scitotenv.2021.147746>.

470 Marcovecchio, A., Behrangi, A., Dong, X., Xi, B., Huang, Y. Precipitation Influence on and Response to Early and  
471 Late Arctic Sea Ice Melt Onset During Melt Season. *International Journal of Climatology*

472 Mayer C, Lambrecht A, Belo` M, Smiraglia C and Diolaiuti G.: Glaciological characteristics of the ablation zone of  
473 Baltoro glacier, Karakoram, Pakistan. *Ann. Glaciol.*, *43*, 123–131, doi: 10.3189/172756406781812087, 2006

474 Niu, H., Kang, S., Wang, H., Du, J., Pu, T., Zhang, G., Lu, X., Yan, X., Wang, S., Shi, X., 2020. Light-absorbing  
475 impurities accelerating glacial melting in southeastern Tibetan Plateau. *Environ. Poll.* *257*, 113541.  
476 <https://doi.org/10.1016/j.envpol.2019.113541>.

477 Rai M., Mahapatra P.S., Gul C. et al., Aerosol Radiative Forcing Estimation over a Remote High-altitude Location  
478 (~4900 masl) near Yala Glacier, Nepal, *Journal of Aerosol and Air Quality Research*, *19*: 1872–1891, doi:  
479 10.4209/aaqr.2018.09.0342, 2019

480 Pepin N C and Lundquist J D 2008 Temperature trends at high elevations: patterns across the globe *Geophys. Res.*  
481 *Lett.* *35* L14701

482 Qian, Y., Flanner, M. G., Leung, L. R. and Wang, W. 2011. Sensitivity studies on the impacts of Tibetan Plateau  
483 snowpack pollution on the Asian hydrological cycle and monsoon climate. *Atmos. Chem. Phys.* *11*, 1929-1948.

484 Qian, Y., Wang, H., Zhang, R., Flanner, M. G., & Rasch, P. J. (2014). A sensitivity study on modeling black carbon  
485 in snow and its radiative forcing over the Arctic and Northern China. *Environmental Research Letters*, *9*(6),  
486 064001.

487 Qu, B., Ming, J., Kang, S. C., Zhang, G. S., Li, Y. W., Li, C. D., Zhao, S. Y., Ji, Z. M. and Cao, J. J.: The decreasing  
488 albedo of the Zhadang glacier on western Nyainqentanglha and the role of light-absorbing impurities, *Atmos.*  
489 *Chem. Phys.*, *14*(20), 11117–11128, doi:10.5194/acp-14-11117-2014, 2014.

490 Quinn, P. K., Bates, T. S., Baum, E., Doubleday, N., Fiore, A. M., Flanner, M., Fridlind, A., Garrett, T. J., Koch, D.,  
491 Menon, S., Shindell, D., Stohl, A., and Warren, S. G.: Short-lived pollutants in the Arctic: their climate impact

492 and possible mitigation strategies, *Atmos. Chem. Phys.*, 8, 1723–1735, doi:10.5194/acp-8-1723-2008, 2008.

493 Ramanathan, V., and Carmichael, G.: Global and regional climate changes due to black carbon, *Nat. Geosci.*, 1,

494 221–227, doi:10.1038/Ngeo156, 2008.

495 Ricchiazzi, P., Yang, S. R., Gautier, C., and Soble, D.: SBDART: A research and teaching software tool for plane-

496 parallel radiative transfer in the Earth's atmosphere, *B. Am. Meteorol. Soc.*, 79, 2101–2114, 1998.

497 Schmale, J., Flanner, M., Kang, S., Sprenger, M., Zhang, Q., Guo, J., Li, Y., Schwikowski, M., Farinotti, D., 2017.

498 Modulation of snow reflectance and snowmelt from Central Asian glaciers by anthropogenic black carbon. *Sci.*

499 *Rep.* 7, 40501. <https://doi.org/10.1038/srep40501>.

500 Vaux, H. J., Jr., Balk, D., Cook, E. R., Gleick, P., Lau, W. K.-M. et al.: *Himalayan Glaciers: Climate Change, Water*

501 *Resources, and Water Security*. National Academies Press, Washington, DC, 2012.

502 Wang, X., Pu, W., Ren, Y., Zhang, X., Zhang, X., Shi, J., Jin, H., Dai, M. and Chen, Q.: Snow albedo reduction in

503 seasonal snow due to anthropogenic dust and carbonaceous aerosols across northern China, *Atmos. Chem. Phys.*

504 *Discuss.*, (September), 1–52, doi:10.5194/acp-2016-667, 2016.

505 Wang, Y., Ma, P.L., Peng, J., Zhang, R., Jiang, J.H., Easter, R.C., Yung, Y.L., 2018. Constraining aging processes of

506 black carbon in the community atmosphere model using environmental chamber measurements. *J. Adv. Model.*

507 *Earth Syst.* 10 (10), 2514e2526. <https://doi.org/10.1029/2018MS001387>.

508 Warren, S. G., and R. E. Brandt.: Optical constants of ice from the ultraviolet to the microwave: A revised

509 compilation, *J. Geophys. Res.*, 113, D14220, doi:10.1029/2007JD009744, 2008.

510 Xu, B., Cao, J., Joswiak, D. R., Liu, X., Zhao, H. and He, J.: Post-depositional enrichment of black soot in snow-

511 pack and accelerated melting of Tibetan glaciers, *Environ. Res. Lett.*, 7(1), 14022, doi:10.1088/1748-

512 9326/7/1/014022, 2012.

513 Yang, S., Xu, B., Cao, J., Zender, C. S. and Wang, M.: Climate effect of black carbon aerosol in a Tibetan Plateau

514 glacier, *Atmos. Environ.*, 111, 71–78, doi:10.1016/j.atmosenv.2015.03.016, 2015.

515 Yasunari, T. J., Koster, R. D., Lau, W. K. M., and Kim, K.: Impact of snow darkening via dust, black carbon, and

516 organic carbon on boreal spring climate in the Earth system, *J. Geophys. Res.-Atmos.*, 120, 5485–5503,

517 <https://doi.org/10.1002/2014JD022977>, 2015.

518 Yasunari, T. J., Bonasoni, P., Laj, P., Fujita, K., Vuillermoz, E., Marinoni, A., Cristofanelli, P., Duchi, R., Tartari, G.

519 and Lau, K. M.: Estimated impact of black carbon deposition during pre-monsoon season from Nepal Climate

520 Observatory - Pyramid data and snow albedo changes over Himalayan glaciers, *Atmos. Chem. Phys.*, 10(14),

521 6603–6615, doi:10.5194/acp-10-6603-2010, 2010.

522 Yao, T., Xue, Y., Chen, D., Chen, F., Thompson, L., Cui, P., Koike, T., Lau, W. K., Lettenmaier, D., Mosbrugger, V.,

523 Zhang, R., Xu, B., Dozier, J., Gillespie, T., Gu, Y., Kang, S., Piao, S., Sugimoto, S., Ueno, K., Wang, L., Wang,

524 W., Zhang, F., Sheng, Y., Guo, W., , Yang, X., Ma, Y., Shen, S. S. P., Su, Z., Chen, F., Liang, S., Liu, Y., Singh, V.

525 P., Yang, K., Yang, D., Zhao, X., Qian, Y., Zhang, Y., & Li, Q. (2019). Recent Third Pole's Rapid Warming

526 Accompanies Cryospheric Melt and Water Cycle Intensification and Interactions between Monsoon and

527 Environment: Multidisciplinary Approach with Observations, Modeling, and Analysis, *Bulletin of the American*

528 *Meteorological Society*, 100(3), 423-444. Retrieved Nov 1, 2021,

529 from <https://journals.ametsoc.org/view/journals/bams/100/3/bams-d-17-0057.1.xml>

530 You Q., Z. Cai, Nick Pepin, Deliang Chen, Bodo Ahrens, Zhihong Jiang, Fangying Wu, Shichang Kang, Ruonan  
531 Zhang, Tonghua Wu, Pengling Wang, Mingcai Li, Zhiyan Zuo, Yanhong Gao, Panmao Zhai, Yuqing Zhang.  
532 Warming amplification over the Arctic Pole and Third Pole: Trends, mechanisms and consequences. *Earth-*  
533 *Science Reviews*, 217: 103625. <https://doi.org/10.1016/j.earscirev.2021.103625>.

534 Zaveri, R., Easter, R., Fast, J., and Peters, L.: Model for simulating aerosol interactions and chemistry (MOSAIC), *J.*  
535 *Geophys. Res.*, 113, D13204, doi:10.1029/2007JD008782, 2008.

536 Zhang, Q., Kang, S., Kaspari, S., Li, C., Qin, D., Mayewski, P. A., and Hou, S.: Rare earth elements in an ice core  
537 from Mt. Everest: Seasonal variations and potential sources, *Atmos. Res.*, 94, 300–312, 2009.

538 Zhang, X. L., Wu, G. J., Kokhanovsky, A., Yao, T. D., and Tong D.: Spectral albedo parameterization for dirty snow  
539 with considering mirco-physicochemical properties of impurities - Part I: Theory and preliminary evaluation,  
540 2016

541 Zhang, Y., Kang, S., Xu, M., Sprenger, M., Gao, T., Cong, Z., Li, C., Guo, J., Xu, Z., Li, Y., Li, G., Li, X., Liu, Y.  
542 and Han, H.: Light-absorbing impurities on Keqikaer Glacier in western Tien Shan : concentrations and potential  
543 impact on albedo reduction, *Sciences in Cold and Arid Regions*, 9(2), doi:10.3724/SPJ.1226.2017.00097. 2017.

544 Zhang Y. L., S. Kang, M. Sprenger, Z. Cong, T. Gao, C. Li, S. Tao, X. Li, X. Zhong, M. Xu, W. Meng, B.  
545 Neupane, X. Qin, M. Sillanpää. 2018. Black carbon and mineral dust in snow cover on the Tibetan Plateau. *The*  
546 *Cryosphere*, 12: 413-431. <https://doi.org/10.5194/tc-12-413-2018>.

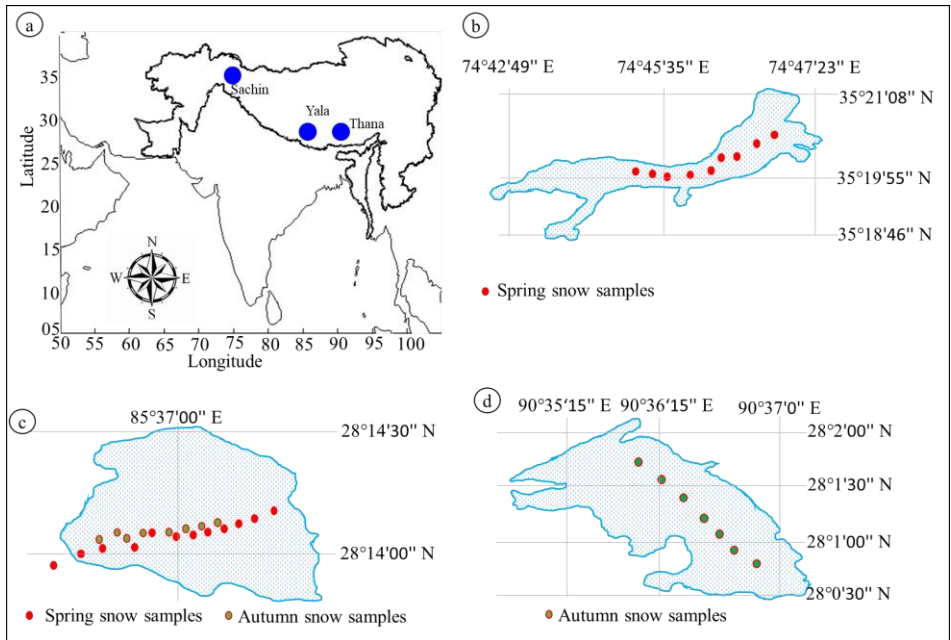
547

548 Zhao, C., Hu, Z., Qian, Y., Ruby Leung, L., Huang, J., Huang, M., Jin, J., Flanner, M. G., Zhang, R., Wang, H., Yan,  
549 H., Lu, Z., and Streets, D. G.: Simulating black carbon and dust and their radiative forcing in seasonal snow: a  
550 case study over North China with field campaign measurements, *Atmos. Chem. Phys.*, 14, 11475–11491,  
551 <https://doi.org/10.5194/acp-14-11475-2014>, 2014.

552

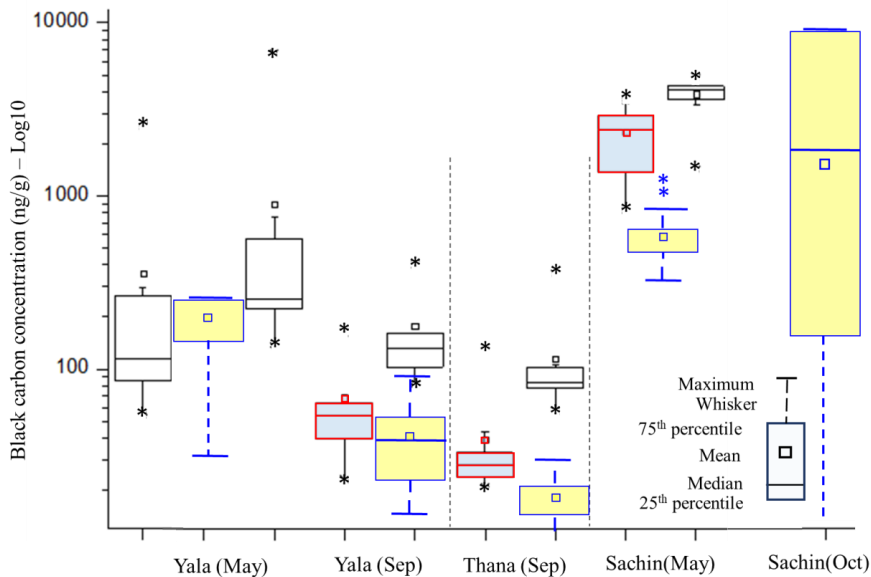
553





554  
555  
556  
557

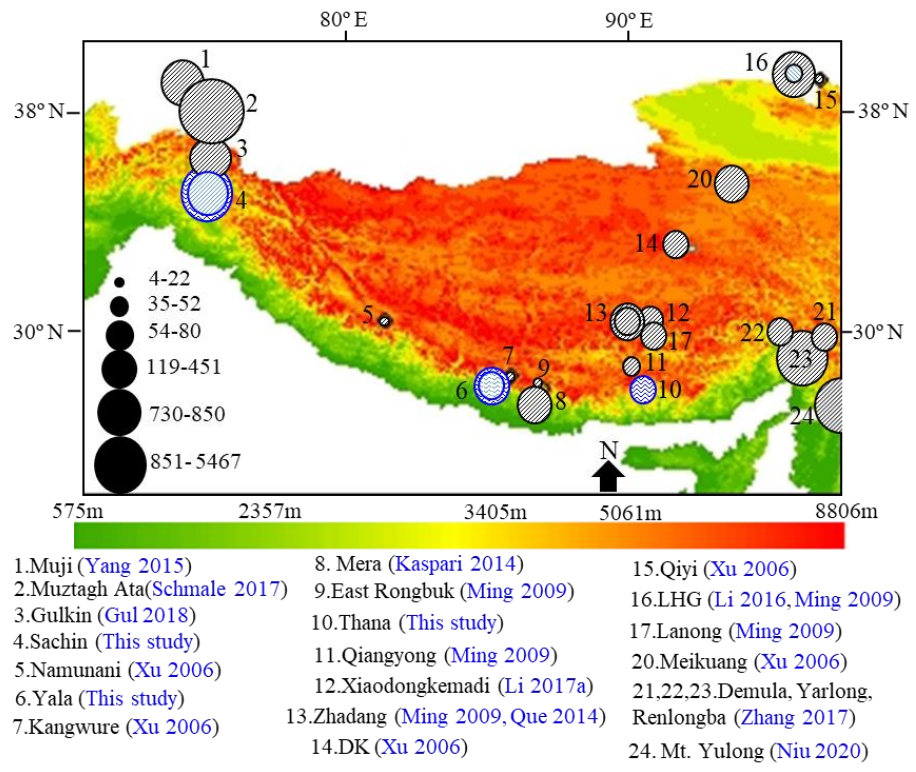
**Fig. 1.** Study area map (a) locations of selected glaciers in Himalaya Karakoram and Hindu Kush region (b) Sachin glacier in Pakistan (c) Yala glacier in Nepal (d) Thana glacier in Bhutan



558

559 | Fig. 2. Whisker plots of black carbon (red box) and organic carbon (black box) concentrations (ng/g<sup>-1</sup>) in snow samples  
 560 | collected from three different glaciers in spring and autumn 2016. The yellow boxes are representing BC content in  
 561 | surface snow from WRF-Chem simulations. Stars (\*) are representing outliers.

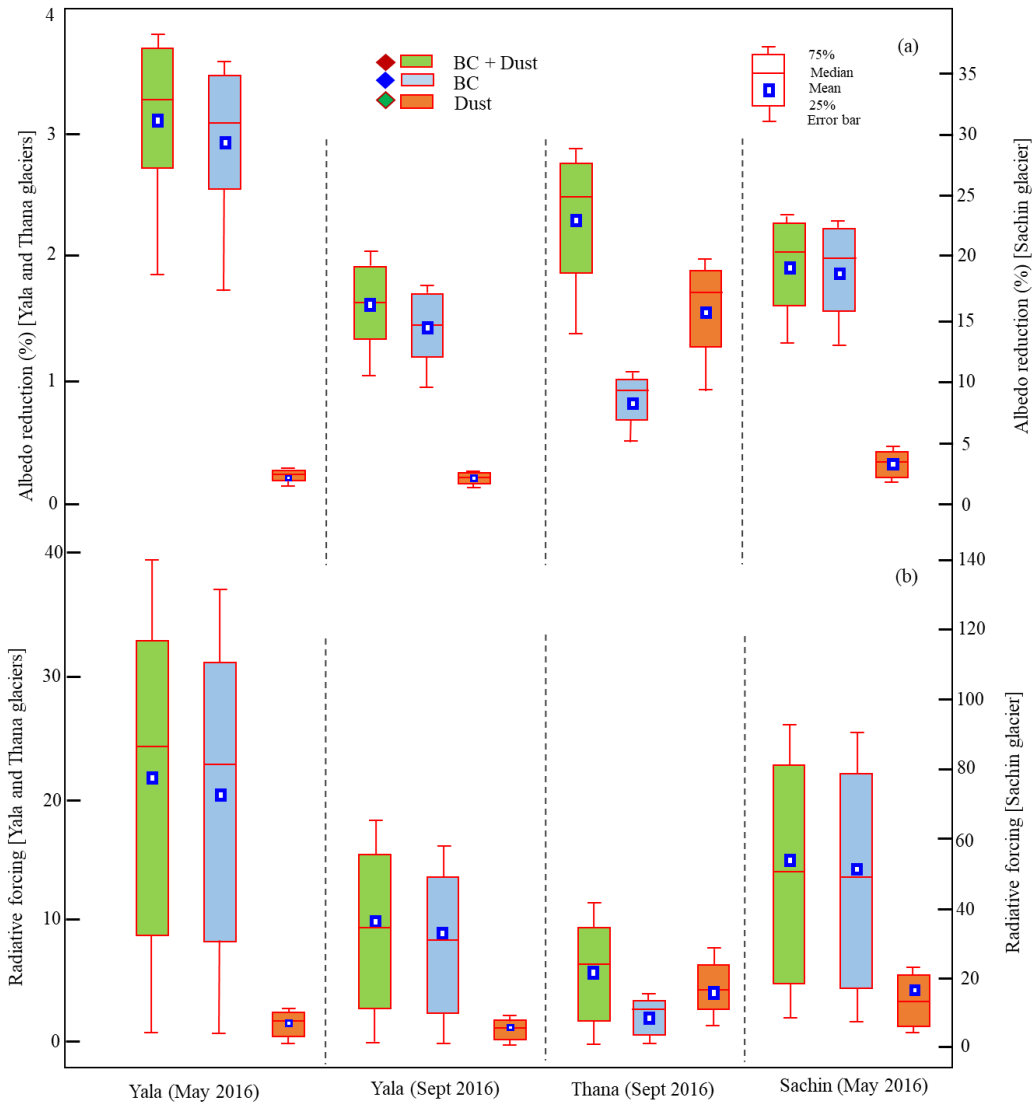
Formatted: Superscript, Highlight



562

563 | Fig. 3. Black carbon concentrations (ng/g) in snow/ice samples in Himalayan, Karakoram and Tibetan Plateau in  
 564 | previous studies (black circles) and this study (blue circles).

565



566

567

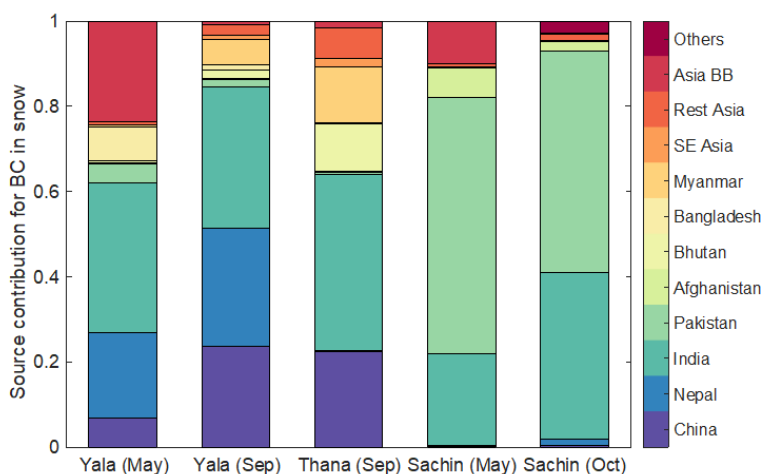
568

569

**Fig. 4. (a) Snow albedo reduction due to black carbon, dust and combined (black carbon and dust) during day time for a range of solar zenith angles. (b) Average instantaneous radiative forcing based on albedo reduction values during day time.**

570

571



572

573 **Fig. 5. Source contributions to BC content in surface snow from WRF-Chem simulations at the three measurement**  
 574 **glacier sites during the measurement periods. Source regions include anthropogenic emissions from China, India, Nepal,**  
 575 **Pakistan, Afghanistan, Bhutan, Bangladesh, Myanmar, Southeast (SE) Asia, and the rest of Asia, as well as Asian biomass**  
 576 **burning (BB) and BC transported from areas outside the study domain (Others).**

577

578

579

580

**Table 1. Snow sampling time and locations from selected glaciers**

Glacier	Lat/Long	Sampling date	Average elevation	Himalayas
Yala (Nepal)	28° 14' 12.25"N, 85° 37' 04.24"E	4 <sup>th</sup> - 7 <sup>th</sup> May 2016	4950 meters	Central
Yala (Nepal)	28° 14' 12.25"N, 85° 37' 04.24"E	29 <sup>th</sup> September 2016	4950 meters	Central
Thana (Bhutan)	28° 01' 22.23"N, 90° 36' 28.72"E	15 <sup>th</sup> September 2016	5400 meters	Central
Sachin (Pakistan)	35° 19' 55"N, 74° 45' 35"E	15 <sup>th</sup> May 2016	3230 meters	Western

581

582

583

**Table 2. Comparison of BC mass concentration, albedo reduction, radiative forcing and potential source regions of pollutants for central and western Himalayan glaciers during the study period**

	Central Himalaya min – max (average)	Western Himalaya min – max (average)	Time period
Monthly mean temperature (°C)	2.05-14.36(10.35) Yala -9.11- 5.68(0.23) Thana	-10.78 - 14.63 (3.57) Sachin	Apr 2015- Oct 2017
Monthly mean precipitation (mm day <sup>-1</sup> )	0.04536 - 41.472 Yala 1.0195 - 50.112 Thana	0.1546 - 5.866 (Sachin)	Apr 2015- Oct 2017
Monthly mean precipitation (mm), during sampling months	(4) Yala + Thana (29) Yala + Thana	(4) Sachin (3) Sachin	Apr 2016 Sep 2016
Elevation of sampling location (meters)	4580-5675 (5127)	3134-3957(3545)	
Observed BC in surface snow (ng g <sup>-1</sup> )	21 – 2529 (~350)	835 – 3545 (~2300)	2016
Albedo reduction (%) due to	0.13-3.82	12.00-24.00	2016

BC particles in snow

Instantaneous radiative forcing  
( $W m^{-2}$ ) due to BC particles

0.0-39.65

0.03 to 96.48

2016

Potential source regions of  
pollutants

3. WRF-Chem simulations

For the Yala site, it is dominated (>50%)  
by anthropogenic emissions from India  
and Nepal for both May and October,  
while the biomass burning contribution  
(>20%) increases largely in May.

For the Thana site, it is dominated (>60%)  
by anthropogenic emissions from China  
and India in September, while  
anthropogenic emissions from Bhutan and  
Myanmar also contribute about 10%,  
respectively.

For the Sachin site, it is predominantly affected  
by anthropogenic emissions from India and  
Pakistan (total contribution >80%), while the  
spring biomass burning only contributes to  
~10% in May.

584  
585